Solar Energy 188 (2019) 1111–1117

Contents lists available at ScienceDirect

Solar Energy

journal homepage: www.elsevier.com/locate/solener

# Uniaxially aligned microwire networks for flexible transparent electrodes using a novel electrospinning set-up

A.A. Yousefi[a], A.R. Mohebbi[a], S. Falahdoost Moghadam[a], S.A. Poursamar[b], L. Hao[c,d]

[a] Energy Division, Iran Polymer and Petrochemical Institute, P.O. Box 14965-115, Tehran, Iran
[b] Biomaterials, Nanotechnology, and Tissue Engineering Group, Advanced Medical Technology Department, Isfahan University of Medical Sciences, P.O. Box 81744-176, Isfahan, Iran
[c] Advanced Manufacturing Research Center for Jewelry, Gemological Institute, China University of Geosciences, P.O. Box 430074, Wuhan, China
[d] Choc Edge Ltd, Innovation Center, Rennes Drive, P.O. Box EX4 4RN, Exeter, UK

ARTICLE INFO

*Keywords:*
Transparent electrode
3D printing
Near-field electrospinning
Solar cell
Flexibility
Conductivity

ABSTRACT

The present work, reports on combination of precise positioning ability of 3D printers with near field electro spinning (NFES) as a low-cost and scalable approach to generate well-aligned, evenly distributed microfiber mask upon flexible substrates coated with metal thin film. Using a combination of annealing thermal treatment and the wet chemical etching of metal layer a flexible transparent electrode is prepared. Using this high speed and large-area printing technique we can overcome the drawbacks of conventional electrospinning such as fiber structural inhomogeneity, random orientation, and non-reproducible results. In addition, the application of more complicated and expensive methods such as lithography or e-beam lithography or nanoimprint lithography can be avoided using this technique. The most important advantage of the reported fabrication method relative to electro-spinning process is the ability to have a special control on the distribution pattern of the electrodes on the surface which can lead to better control over the ratio of conductivity and transparency of the surface.

## 1. Introduction

Transparent electrodes, indispensable in displays and solar cells, are currently dominated by indium tin oxide (ITO) films although high price of indium, brittleness of films, and high vacuum deposition are limiting their applications.

Ultra-thin layers of alternative materials such as conducting polymers (Na et al., 2008), carbon nanotubes (Pasquier et al., 2005), graphene (Wang et al., 2008) and metal nanowire grids (Kang et al., 2010) show unique electronic transport and optical properties. In particular they can be used as low cost and efficient transparent electrodes in optoelectronic devices including touch screens (Lee et al., 2012), organic light-emitting diodes (OLEDs) (Zhang et al., 2006), electronic displays (Hecht et al., 2011), and solar cells (Nogi et al., 2015) to replace expensive and brittle ITO.

The challenge of optimizing the conductivity properties of such materials is network formation methods. A low junction resistance between nanostructures is important for decreasing the sheet resistance and the junction resistances between deposited electrodes can increase without coherent order within the network structure.

Recently, solution-processed networks of nanostructures such as carbon nanotubes (CNTs), graphene, and silver nanowires have attracted great attention as replacements. Several research studies are reported the fabrication of transparent conductive polymer sheets for applications in electronics using electrospinning technique as a low-cost and scalable fabrication process (Wang et al., 2008). Recently, a metal mesh micro/nanoweb have been demonstrated to be a promising candidate for fabricating of transparent conducting electrodes (Fuh and Lien, 2013), because of its high conductivity and high transmittance. It composes of a hardly visible or sometimes an invisible metal mesh that can be fabricated onto any glass or plastic surface. This two-dimensional micro/nanostructure thin metal layer can be created from almost any types of metal such as silver, aluminum, platinum, copper or nickel. Azuma et al. fabricated a transparent and conductive Al nanowire networks by wet chemical etching of an Al thin film with an electrospun polymer nanofiber mask (Azuma et al., 2014). Fuh et al. used electrospun nanofiber templates and the dry pattern transfer process to obtain a random metal nano/microwire networks to be used as flexible transparent electrodes (Fuh and Lien, 2013). Cui et al prepared a transparent electrode, composed of a random and free-standing metallic nanotrough network, with a process involving standard electrospinning and metal deposition (Wu et al., 2013; Huh et al., 2016).

However, all these works state that the electrospinning is a random and non-controllable process, so that, the orientation and distribution

*E-mail address:* a.yousefi@ippi.ac.ir (A.A. Yousefi).

https://doi.org/10.1016/j.solener.2019.07.007
Received 16 December 2018; Received in revised form 19 June 2019; Accepted 1 July 2019
Available online 09 July 2019

of the polymer nanofiber template are difficult to control, and there is little to none control over fabrication process in electrospinning process which can results in higher electrical resistance and lower transparency and sample-to-sample variation of electrode performance may not be avoided.

Recently a new fabrication method is reported as a combination of additive manufacturing and electrospinning which can provide significantly higher order into the prepared structure (Wang et al., 2008). In many literatures, this method is referred to as *mechano electrospinning, electro hydro dynamic printing* (*EDH*) (Yin et al., 2018) or *near-field electrospinning* (*NFES*) (Min et al., 2013). NFES is a powerful technique which recently developed to print out uniaxially aligned fibers with precise control of fiber size and placement (Min et al., 2013; Fuh and Lu, 2014). The key advantage of this technique lies in the low applied voltage and short electrode-to-collector distance which provide better fiber deposition controllability. Despite many advantages of NFES in fabrication of flexible and nanoscale electronics such as high-speed, large-area printing of aligned fibers, to the best of our knowledge this technique has not been reported for manufacturing polymeric flexible transparent electrodes.

The present work reports on combination of precise positioning ability of 3D printers with NFES as a low-cost and scalable approach to generate well-aligned, evenly distributed microfiber mask upon flexible substrates coated with metal thin film; Using the wet chemical etching of metal layer a flexible transparent electrode is prepared. The electrodes are characterized using conductivity, bending, and transparency tests.

## 2. Materials and methods

### 2.1. Materials

Polystyrene (PS, 1440 grade) with molecular weight of 240,000 $g \cdot mol^{-1}$ was purchased from Tabriz Petrochemical Company (TPCO, Tabriz, Iran). Adequate amount of PS was dissolved in dimethylformamide (DMF, Merck, Germany) at 70 °C for 15 min in order to yield 30% w/v solution. The viscosity of these solutions was measured at room temperature by using a digital rotational viscometer. In order to optimize the viscosity of the solution, 10% and 0.01% of $FeCl_3$ and single walled carbon nanotube (SWCNT) with respect to PS weight was added to the solution, respectively.

### 2.2. NFES printing of microscale fiber

As shown in Fig. 1, a custom-made electro-hydrodynamic 3D printing platform based on Choc Creator 1 platform (Choc Edge Ltd, UK) was used to fabricate well-aligned microfiber mask upon flexible substrates. PS solution was loaded into a 10 ml syringe. The printing nozzle with an internal diameter of 455 µm was connected with the positive terminal of a DC voltage generator. The voltage was regulated at 24 V. In this study, a 70 × 70 mm polyethylene terephthalate (PET) was sputter coated (K450X Sputter Coater, EMITECH, UK) with a thin layer of gold (~60 nm, sputter time 2 min at 20 mA), then was mounted on the moving stage as the collector. The collector was connected with the negative terminal of the DC voltage generator. The nozzle-to-collector distance was kept 0.2 mm and the moving speed was 15 $mm \cdot s^{-1}$.

### 2.3. Preparation of printed electrodes

The PS fibers were printed onto the gold-coated PET (Au-PET) collector producing the dimension-specific pattern. In order to maximize the contact between the printed pattern of PS fibers and the underneath Au-PET, the prepared patterns were annealed at 200 °C for 20 min after which etching of the gold coating was carried out. The printed PS pattern functions as a temporary mask on Au-PET substrate allowing control removal of Au from the surface by wet etching and

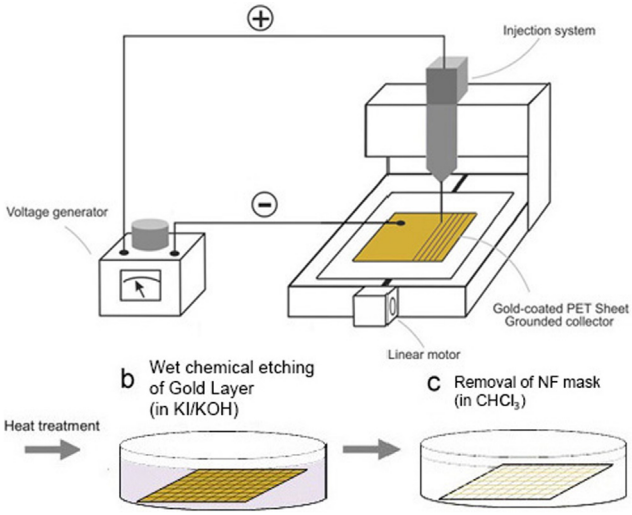


**Fig. 1.** The schematic view of NFES printing of microfibers. (a) NFES was used to produce well-aligned PS micro fibers onto PET substrate, (b) Wet chemical etching selectively remove Au coating between the PS fibers whilst the PS fibers act as temporary mask protecting the Au underneath. (c) PS fibers are removed leaving an Au network pattern exposed.

preserving the Au located underneath the printed PS fibers. The etching was performed using KI/KOH solution with concentration of 2:1 in 20 ml di-ionized water for 90 s. The samples were excessively washed with de-ionized water and eventually the printed PS fibers were removed from the surface with formaldehyde wipe exposing the remaining Au fibers remaining underneath.

### 2.4. Conductivity measurements

The sheet resistance of the transparent PET electrodes in a 25 × 20 mm square was measured using the 4-probe device in 2-point probe mode (Sanat Nama Javan, FPP-SN-554, Iran). The electrical contacts were made by pressing the probe tips on the 3 random spot on transparent PET electrodes. The current values were modulated from 10 µA to 0.7 mA while recording the corresponding voltage and producing a linear diagram the slope of which was reported as resistance of the sample in Ohm.

In order to study the impact of sample length on conductivity of the electrodes, above mentioned custom-made two-probe electrode was used. The electrodes with desirable dimensions were cut into rectangle shapes and the probes were placed at the length of cut samples, similarly the sample resistance was reported as the slope of voltage-current diagram.

### 2.5. Transparency measurements

The optical transparency at a wavelength between 200 and 1100 µm was measured using a UV–visible–near infrared spectrophotometer (SPECORD 250, Analytik Jena, Germany) in transmittance mode using 0.5 nm slit and the sample size of 25 × 25 mm.

### 2.6. Bending test

A 20 × 20 mm electrode was cut and was fixed between two holders. The Bending test was performed at 18 $mm \cdot s^{-1}$rateand under the lateral dislocation of 11 mm causing a matching radius bending. The impact of 10,000 bending cycles on the conductivity of the samples was studied. The bending test was carried out on the same custom-made printer used for NFES by removing the extrusion section and installing clamps to hold the electrode specimen. The printer was programmed to oscillate 11 mm in Y-direction for up to 2500 cycles. The sheet

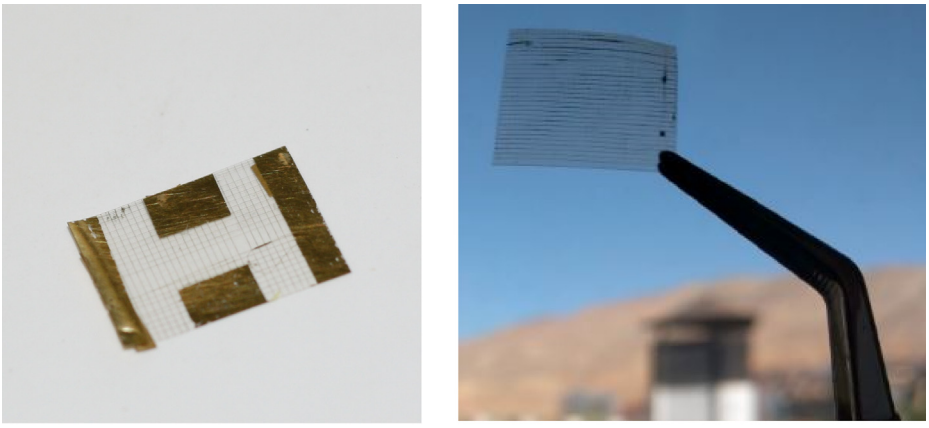

(a) (b)

**Fig. 2.** (a) The naked-eye view of the 2 × 1.5 cm electrodes. The solid Au coating on the left and right sides and the mid-top and bottom sides of the electrodes are preserved by masking using Sellotape®. These areas were acting as 2-probe conductivity tests. (b) A representation of optical clarity of electro-printed sample.

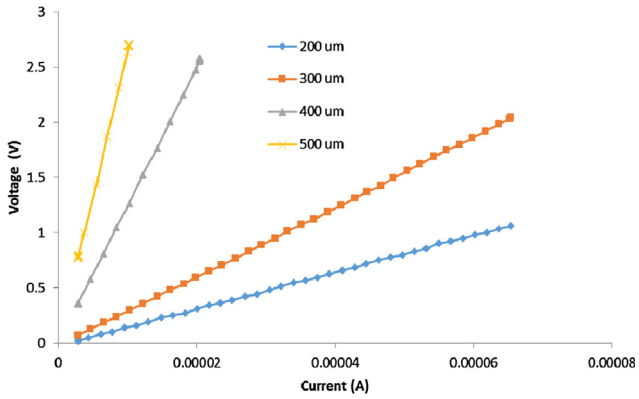


**Fig. 3a.** The sheet resistance ($R_s$) of the prepared electrodes as a function of lateral distance between the printed fibers (electrode distance 25 mm). The linear slope of the diagram is representative of sheet resistance ($R_s$) (Azuma et al., 2014). The higher slope represents higher $R_s$ values. Decreasing the lateral distance between the printed fibers reduced the $R_s$ value.

resistance was measured using the method described in previous section and then test was continued for other 25,000 cycles for the total cycles of 10,000.

### 2.7. Surface analysis

Microstructure analyses were carried out using scanning electron microscope (SEMVEGA/TESCAN, Czech Republic). The samples were sputter coated (K450X Sputter Coater, EMITECH, UK) with a thin layer of gold (~60 nm, 3 fold sputter time 2 min at 20 mA) to improve the conductivity of the surface. The samples were studied under 20 kV acceleration voltage.

## 3. Results and discussion

Recently, metallic micro/nanowebs have been demonstrated to be a promising candidate for fabricating of transparent conducting electrodes, due to their high conductivity and high transmittance. The conductivity of metallic layer depends not only on the type of metallic materials but, on geometrical design of the mesh, whereas the transparency depends only on the design of mesh geometry. The high conductivity and transparency of metal mesh wires are attributed to their uniform and interconnected network which leads to a decrease in junction contact resistance and increase in light transmittance through open area surfaces. Various fabrication methods have been employed to develop micro/nano mesh structures, such as e-beam lithography or nanoimprint lithography (Otagawa et al., 1995), UV lithography and wet etching (Kim et al., 2015), electrospinning and wet etching (Azuma et al., 2014).

Among these, conventional electrospinning has exhibited a less expensive and complicated method and is stable for large-area application. Electrospinning is an attractive and viable process to fabricate micro/nanoscale fibrous mats. However, the nanofibers fabricated by electrospinning exhibit poor control over fiber arrangements, large surface roughness and length inhomogeneity which commonly caused high surface resistivity and low transparency. Therefore, for important application of transparent electrode for advanced electrical devices highly aligned and well-ordered web of fibers are required.

Application of NFES for producing fully regular and predefined patterns of conductive micro-wires on PET sheets while keeping it transparent is to be discussed. In Fig. 2a a representative naked-eye view of the prepared electrodes and in Fig. 2b the optical clarity of the electro-printed are shown. To attain the goal of producing a transparent

**Table 1**
Sheet resistance (Rs, Ω/sq) for different 500 μm samples at various electrode separations (ES). A typical value for ITO (50 nm thick) is 790 ohm/sq (Mazur et al., 2010).

| ES (mm) | Sample 1 | Sample 2 | Sample 3 | Sample 4 | Sample 5 | Sample 6 | Sample 7 |
|---|---|---|---|---|---|---|---|
| 0.5 | | | | 182 | | | |
| 0.6 | 154 | 610 | | | | | |
| 1 | 250 | 721 | 182 | | | | |
| 1.5 | | | | 271 | | | 72.6 |
| 1.6 | | | | | | 284 | |
| 2 | | | 240 | | | | |
| 2.7 | | | | | 635 | | |

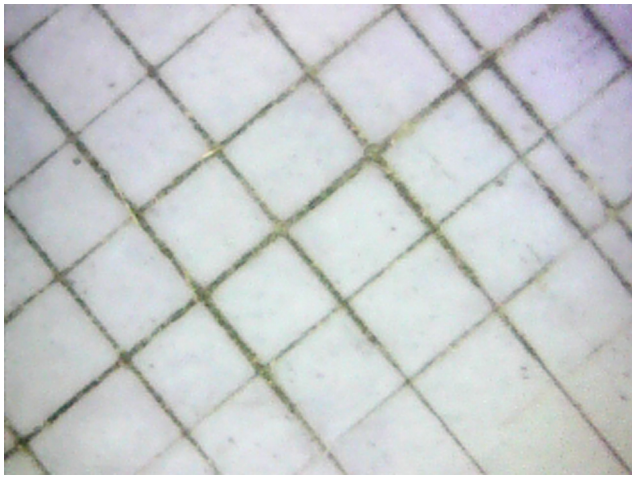

**Fig. 3b.** Optical presentation of typical irregularity in the imprinted 500 µm web (broken fibers and incorrect lateral distances).

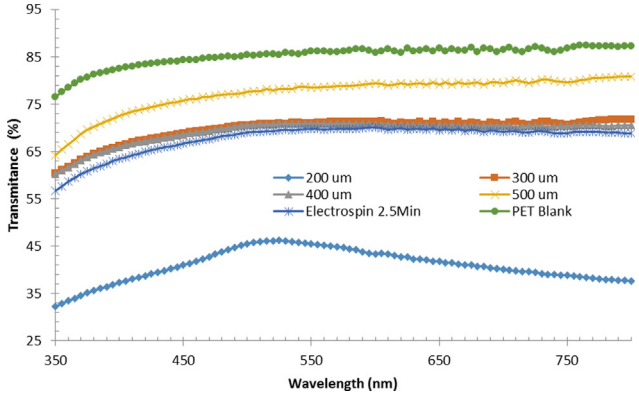


**Fig. 4.** Transparency of prepared electrodes as a function of lateral distance between the printed fibers. The transparency is compared with electrospun samples. As the printed fiber masks grew closer to each other the transparency of the samples were reduced. This reduction was the most for electrodes with lateral distance 200 µm.

and conductive electrode the conductivity of the electrodes should be checked at first. Fig. 3a represents the sheet resistance ($R_S$) of the printed electrodes as a function of fibers lateral distance. With decreasing this distance the number of fibers per unit length of the electors will increased and as a result the $R_S$ value decreased (as represented by the slope of voltage-current curve). The values of $R_s$ are reported in Table 1. As seen, the sheet resistance varies with the electrode separation distance. This could be assigned to some irregularities and no-contact points (Fig. 3b). This is a drawback of the hardware used and is to undergo some improvements.

However, the transparency of the samples was noticeable reduced as a result of reducing the lateral distance between printed fibers. Fig. 4 shows the impact of increasing the density of printed fibers on transparency of the electrodes. Fig. 4 also compare the printed samples transparency with prepared electrodes with electrospinning method according to the method reported by Azuma et al. (Azuma et al., 2014). The printed substrates of electrode with lateral distance of 500 µm exhibited constant transmittances over the whole visible wavelength range of 400–700 µm. These samples showed over 75% transparency which is lower than the reported value for ITO films and higher than the reported values for electrodes prepared from Cu nanofibers (Zhang et al., 2006) and single walled carbon nanotube (Na et al., 2008). Relative to electrospun electrodes the printed samples with 500, 300 and 200 µm lateral distance showed higher, similar, and lower transparency than electrospun electrodes, respectively. As mentioned above, the electrospinning method has little or no control over the alignment of the mask fibers which significantly reduces the transparency. Fig. 4 shows that printed samples only with lateral distance of 500 µm had higher transparency relative to that of electrospun samples. The sample printed with lateral distance of 400 and 300 µm had similar transparencies to that of electrospun samples. The transparency of the samples with 200 µm lateral distance was even lower that of electrospun sample (Electrospin 2.5 min). Scanning electron microscopy was used to confirm the alignment and the orderly distribution of Au wires on the surface of PET sheets and the impact of using masks with smaller lateral distance on the electrode characteristics. Another interesting observation for the prepared electrodes as compared with ITO counterparts is their almost a constant transparency in same wavelength range. The transparency of ITO electrode changes extensively in this frequency region (Askari et al., 1409). Another important point is that ITO electrodes shows conductive layer thickness dependency (Gao et al., 2008) which is minimized in the case of the prepared electrodes.

Fig. 5 shows 2D networks of Au microfibers with lateral distance of

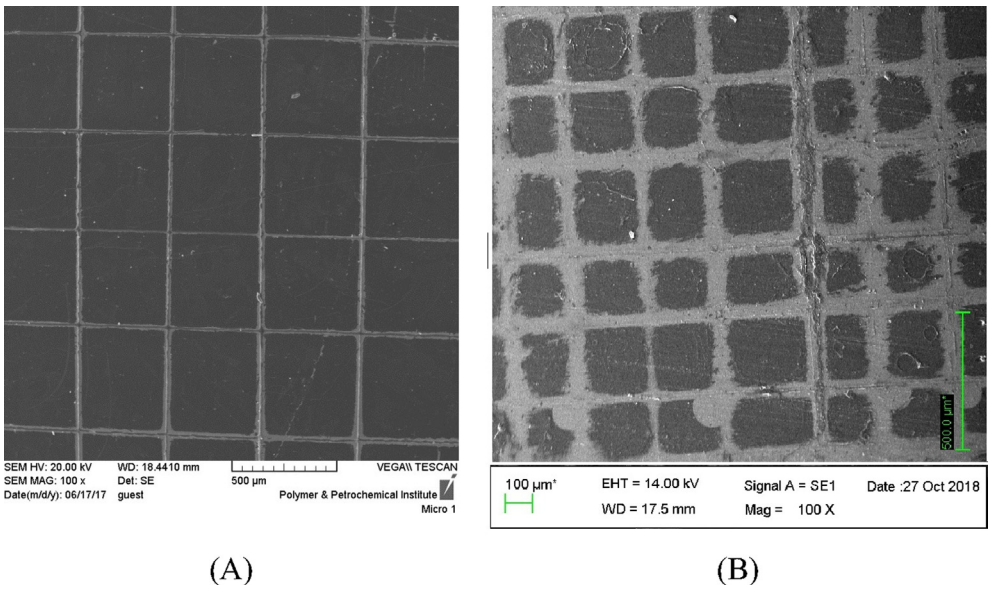


**Fig. 5.** The impact of printed fiber lateral distance on the alignment of Au electrodes on the platform. (A) The printed electrode with lateral distance of 500 µm, (B) the printed electrode with lateral distance of 200 µm. Reducing the lateral distance between the printed fiber mask had led to les clear resolution of Au fibers on the final product.

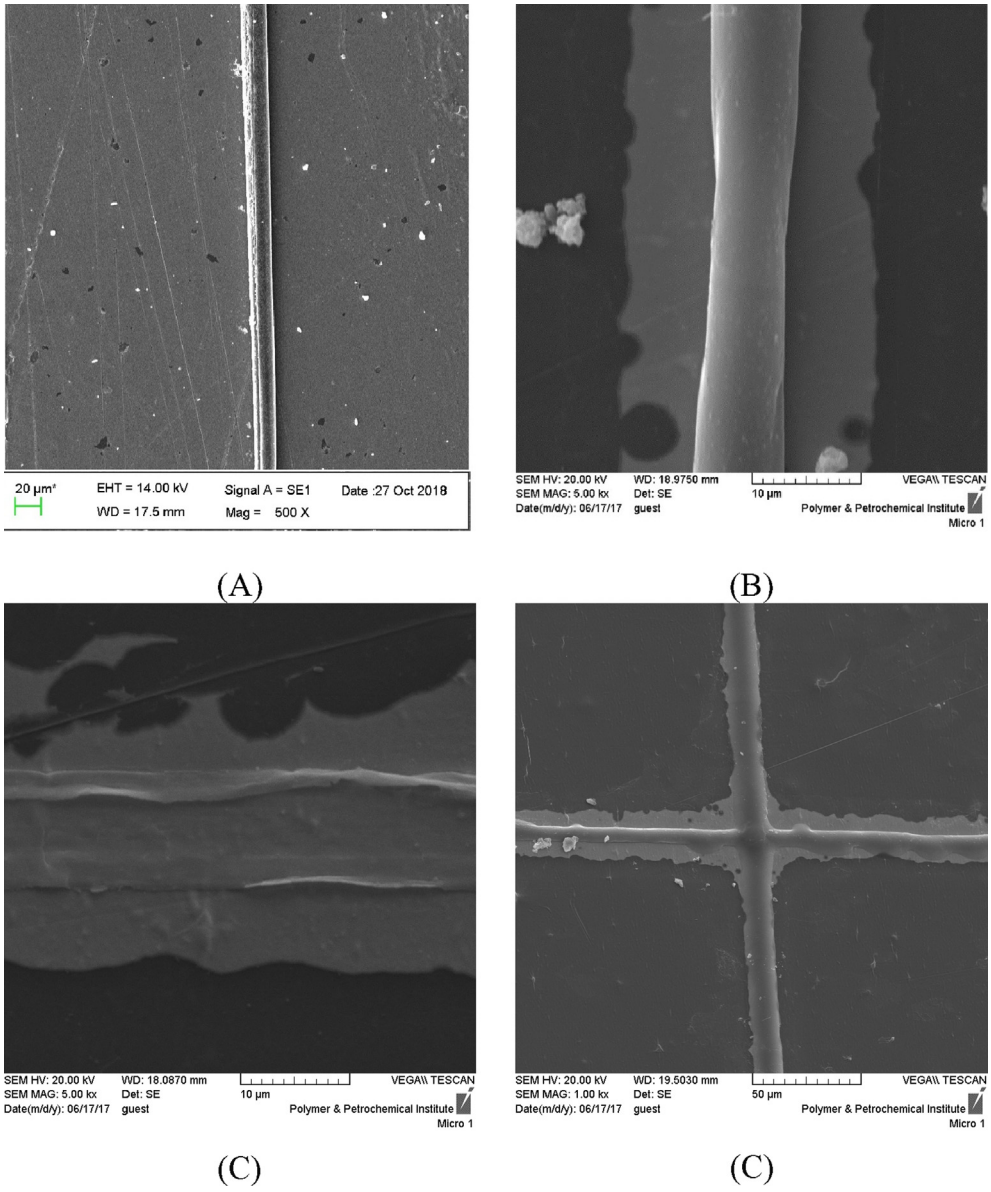


**Fig. 6.** the progress of microstructure during the manufacturing of electrodes; (A) A single PS electrode printed onto Au substrate, (B) The boundary of Au substrate preserved under PS fiber; (C) A high magnification view of the final electrode after removal of PS fiber be means of Chloroform; (D) the impact of annealing on PS fiber and spreading of fiber onto Au substrate.

500 and 200 µm of printed fibers. Increasing the number of printed PS fibers on the substrate by reducing the lateral distance between them, had caused the final electrode to have lower resolution (Fig. 5B). This should be the main reason behind the reduction of transparency which is reported in Fig. 4. In our studies, number of issue acted as artifacts in the manufacturing process. As discussed in the materials and methods section, the printed PS fibers act as temporary mask for the underneath Au coating protecting them against the chemical etchant during the wet etching step. Fig. 6A–C show a single printed fiber before and after etching and after removal of PS mask by means of chloroform solvent. Comparing Fig. 6A–C show that the boundary of etching the Au coating does not completely match the printer fiber diameter. It appears that the PS fibers have a zone of inhibition which prevents the etchant chemical complete contact with Au underneath coating at the immediate vicinity of the fibers.

In addition to apparent inhibition zone of PS fiber, as can be seen in Fig. 6D the polystyrene masks become fluid and spread over the Au surface at 200 °C during annealing step of fabrication. This phenomenon can increase the impact of fiber masking on the Au etching especially at more compact and dense printing patter as seen in Fig. 5B. In sum the combination of inhibition zone of PS fibers during wet etching step (Fig. 6B) and the partial melting of the PS fibers during annealing step of manufacturing (Fig. 6D) will make this manufacturing process less suitable for the printing pattern with lateral distance lower than 500 µm by making the final product less transparent. It appears that considering the practical limitations of this method, there is an optimum balance between the transparency and the conductivity of the surface. The conductivity of the surface has a direct relation with the number of available electrode per square unit of the surface, whereas the transparency of the surface has indirect correlation with the number of available electrode on surface. It appears that 500 µm lateral distance between the printed PS fibers is an optimum value at this printing setup. Hence for applying functional bending tests, only 500 µm samples were chosen. Fig. 7 shows the impacts of bending test on conductivity and physical morphology of the prepared electrodes.

Fig. 7-A shows the impact of bending cycles on the $R_s$ values of the prepared electrodes. (S1 video shows the bending test process in action). The electrode test samples showed desirable resilience during

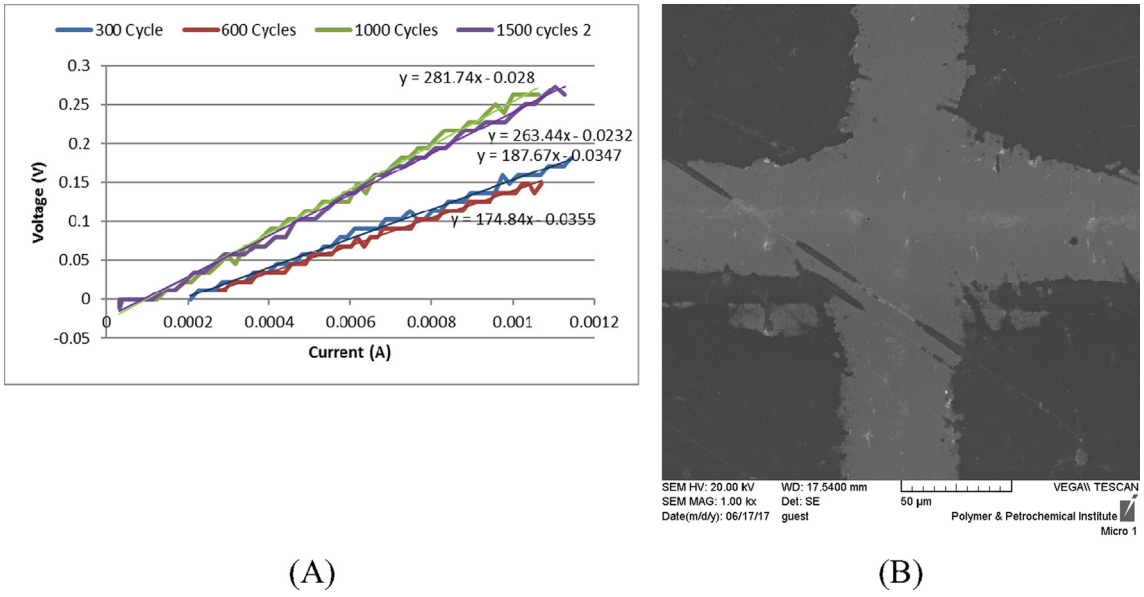


**Fig. 7.** The impact of bending cycles on the sheet resistance ($R_s$) of the prepared electrodes with 500 µm lateral distance; (A) as a function of number of applied bending cycles, (B) The impact of bending cycles on the microstructure morphology of the prepared electrodes.

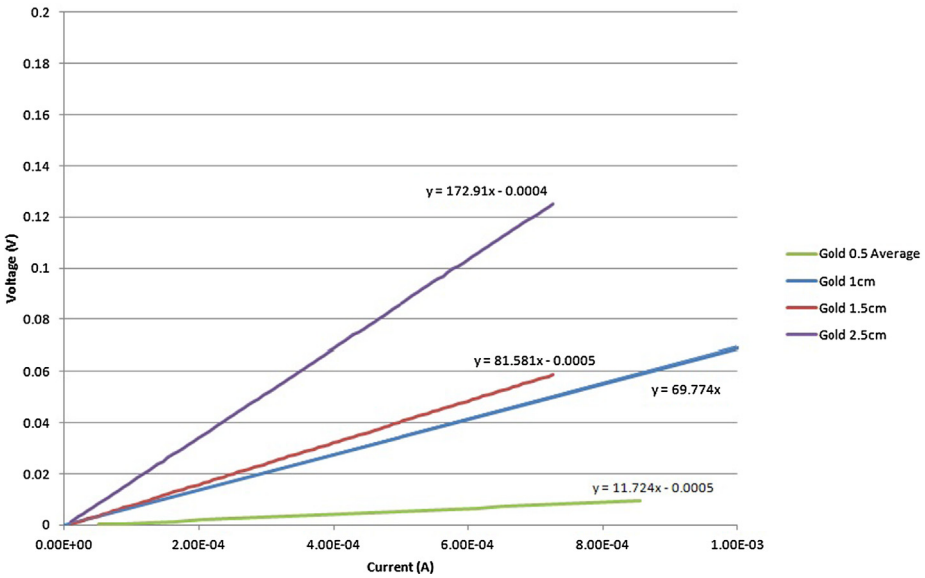


**Fig. 8.** The impact of electrode size on the conductivity of the samples. The increase of electrode size from 5 mm to 25 mm increases the $R_S$ values from 11.75 ohm/sq to 172.91 ohm/sq, respectively.

bending and the electrodes $R_s$ values remain steady up to 600 cycles beyond which the $R_s$ value begins to increase. Upon morphology examination it was shown that the electrode surfaces were shown formation of cracks and partial discontinuity after 1000 bending cycles. A representative view of such discontinuity is shown is Fig. 7-B.

Another practical aspect that deemed important to investigate is the impact of electrode length (size) on the sheet resistance. Fig. 8 shows the change in $R_S$ values of electrodes with lateral distance of 500 µm as a function of electrode size (the electrodes were cut into rectangular shapes and the $R_S$ values were recorded by measuring the conductivity along each side). As shown in Fig. 3b, this changes in $R_s$ with electrode distance is produced due to some defects in fiber array. These defects are produced during printing and etching. Optimized printing and etching processes will lead to less electrode width dependency of $R_s$.

## 4. Conclusion

We have demonstrated that transparent and conductive Au microfiber network can be printed by combination electroprinting and the wet chemical etching of 45 nm thick Au thin film with electroprinted polystyrene mask. This method can be applied to the fabrication of microfibers network with desirable design and it allows the wire length to be controlled. At our current experimental setup the 500 µm lateral distance between the printed fibers was shown to be optimal balance between transparency and conductivity. However, it was shown that printing closer PS fibers with shorter lateral distance between fibers is technically possible, however further optimization in annealing and wet etching steps are required. The impact of annealing temperature on the resolution of printed electrodes should be more closely studied. The impact of duration and concentration of etching solution on the inhibition zone should be investigated in order to obtain more conductive and at the same time transparent electrodes.

## Acknowledgement

The authors wish to acknowledge the technical support of Choc Edge Ltd. in this research study. The printing technology used in this study is based on Choc Creator 1 machine developed by Choc Edge Ltd (UK).

## Appendix A. Supplementary material

Supplementary data to this article can be found online at https://doi.org/10.1016/j.solener.2019.07.007.

## References

Askari, H., Fallah, H.R., Askari, M., Charkhchi Mohmmadieyh, M., 2014. arXiv:1409.5293 [cond-mat.mtrl-sci].
Azuma, K., Sakajiri, K., Matsumoto, H., Kang, S., Watanabe, J., Tokita, M., 2014. Mater. Lett. 115, 187–189.
Fuh, Y.K., Lien, L.C., 2013. Nanotechnology 24, 55301–55308.
Fuh, Y.-K., Lu, H.-Y., 2014. J. Micro/Nanolithography, MEMS, MOEMS 13, 043014.
Gao, M.-Z., Job, R., Xue, D.-S., Fahrner, W.R., 2008. Chin. Phys. Lett. 25, 1380–1383.
Hecht, D.S., Hu, L., Irvin, G., 2011. Adv. Math. 23, 1482–1513.
Huh, J.W., Lee, D.K., Jeon, H.J., Ahn, C.W., 2016. Nanotechnology 27, 475302.
Kang, M.G., Park, H.J., Ahn, S.H., Guo, L.G., 2010. Sol. Energy Mater. Sol. Cell 94, 1179–1184.
Kim, W.K., Lee, S., Lee, D.H., Park, I.H., Bae, J.S., Lee, T.W., Kim, J.W., Park, J.H., Cho, Y.C., Cho, C.R., Jeong, S.Y., 2015. Sci. Rep. 5, 10715.
Lee, J., Lee, P., Lee, H., Lee, D., Lee, S.S., Ko, H., 2012. Nanoscale 4, 6408–6414.
Mazur, M., Kaczmarek, D., Domaradzki, J., Wojcieszak, D., Song, S., Placido, F. (Eds.), October 2010. Proceedings of 8th International Conference on Advanced Semiconductor Devices and Microsystems, ASDAM 2010. IEEE.
Min, T.W., Kim, S.Y., Kim, T.S., Cho, B.J., Noh, H., Yang, Y.Y., Cho, H., Lee, J.H., 2013. Nat. Commun. 4, 1773–1781.
Na, S.I., Kim, S.S., Jo, J., Kim, D.Y., 2008. Adv. Math. 20, 4061–4067.
Nogi, M., Karakawa, M., Komoda, N., Yagyu, H., Nge, T., 2015. Sci. Rep. 5, 17254–17260.
Otagawa, T., Madou, M.J., Wachsman, L.A., 1995, US Patent 5403680.
Pasquier, A.D., Unalan, H.E., Kanwal, A., Miller, S., Chhowalla, M., 2005. Appli. Phys. Lett. 87, 203511.
Wang, X., Zhi, L., Mullen, K., 2008. Nano Lett. 8, 323–327.
Wu, H., Kong, D., Ruan, Z., Hsu, P.C., Wang, S., Yu, Z., Carney, T.J., Hu, L., Fan, S., Cui, Y., 2013. Nat. Nanotechnol. 8, 421–425.
Yin, Z., Huang, Y., Duan, Y., Zhang, H., 2018. Electrohydrodynamic Direct-Writing for Flexible Electronic Manufacturing. Springer.
Zhang, D., Ryu, K., Liu, X., Polikarpov, J., 2006. Nano Lett. 6, 1880–1886.